Journal of Energy Storage 29 (2020) 101381

Contents lists available at ScienceDirect

Journal of Energy Storage

journal homepage: www.elsevier.com/locate/est

Corrosion evaluation of eutectic chloride molten salt for new generation of CSP plants. Part 2: Materials screening performance

Angel G. Fernández*, Luisa F. Cabeza

GREiA Research Group INSPIRES Research Centre, Universitat de Lleida, Pere de Cabrera s/n, 25001, Lleida, Spain

ARTICLE INFO

Keywords:
Concentrated solar power
Thermal energy storage
Corrosion mitigation
Chloride molten salt
Nickel base alloys

ABSTRACT

The operating temperature of a steam turbine is limited to 565 °C by the molten nitrate heat-transfer fluid; therefore, molten-salt CSP technologies require alternative salt chemistries such as chloride. The prevention of high-temperature corrosion on containment materials plays a critical role, and a corrosion mitigation plan is needed to achieve the target plant lifetime of 30 years. This paper performed a materials screening test, using a eutectic ternary chloride molten salt, composed by 20.4 wt. % KCl + 55.1 wt. % $MgCl_2$ + 24.5 wt. % NaCl, in stainless steel (AISI 304) and two Ni base materials (Inconel 702 and Haynes 224). The corrosion mechanism and corrosion rates were obtained through electrochemical impedance spectroscopy (EIS). Ni base alloys showed a protective scale layer during 8 hours of immersion with a corrosion rate of 6.34 mm/year (In702) and 3.12 mm/year (HR224). Monitoring corrosion results were confirmed by scanning electron microscopy (SEM) and X-ray diffraction (XRD), obtaining alumina and chromia protective layers.

1. Introduction

In the last years, an opportunity to obtain higher power-generation efficiencies by integrating high temperature thermal energy storage materials was identified. To achieve this integration, CSP needs to operate at temperatures above 550 °C, which requires advanced high-temperature heat-transfer fluids in the range of 550 °C to 750 °C [1]. The selection of a high-temperature molten-salt is needed, as well as the need to understand its impact on containment materials, to achieve acceptable strength, durability, and cost targets at these high temperatures [1]. Molten chlorides are considered good candidates since they present low cost and high decomposition temperatures. However, these molten salts introduce a set of technological and engineering challenges because of their very corrosive nature on typical containment materials. Corrosion mitigation approaches were investigated [2–6] and the selection of high resistance materials in this environment needs to be addressed. Different materials were tested in the literature in contact with chloride molten salts [4,6–11]. Vidal et al. [3] established the corrosion produced by a mixture composed by 35.59 wt.% $MgCl_2$ – 64.41 wt.% KCl at 700 °C in Ni base alloys. Table 1 shows the results obtained in In702 and HR224.

It is important to highlight that in that study In702 and HR224 alloys were pre-oxidized in zero air (ZA) at 1050 °C during 4 h to generate an alumina protective layer before the corrosion test was carried out.

Ding et al. [12] studied the hot corrosion behaviour of three commercial alloys (310SS, In800H, and HastelloyC270) in the eutectic $MgCl_2$/NaCl/KCl mixture at 700 °C for 500 h. Regarding corrosion resistance, Hastelloy showed better behaviour (79 μm/year) compared to Inconel (364 mm/year) and 310SS (1581 μm/year).

Nevertheless, it is difficult to compare these results from different authors since different thermal purification treatments were carried out before the corrosion test. Thermal treatments are key for corrosion mitigation and a standard procedure must be developed to follow same criteria in this research field.

A specific thermal treatment during the melting process was defined in a previous research [13] in order to reduce the corrosive impurities present in commercial chloride molten salts, especially in $MgCl_2$, following different isothermal steps and dwelling times: 70 °C (2 h)–117 °C (2 h)–145 °C (4 h)–190 °C (4 h)–227 °C (4 h)–300 °C (4 h)–450 °C (3 h)–600 °C (1 h)–720 °C. The easiest way to prevent the contamination of O_2 and H_2O is drying the hygroscopic $MgCl_2$ salt and parameters for the purification treatment were determined from the vapour-pressure curve of hydrated $MgCl_2$. Krammer et al. [14] presented a method that lixiviates the oxides/hydroxychlorides from KCl/$MgCl_2$/NaCl by selective solubility, followed by titration to obtain MgO/MgOHCl content". The use of an inert atmosphere (N_2) is key for avoid catastrophic corrosion in contact with chloride molten salts, nevertheless, it is important to highlight the formation of protective layers in the alloy

* Corresponding author.
E-mail address: angel.fernandez@udl.cat (A.G. Fernández).

https://doi.org/10.1016/j.est.2020.101381
Received 2 August 2019; Received in revised form 10 March 2020; Accepted 16 March 2020

Table 1
Corrosion data from EIS tests of In702 and HR224 pre-oxidized in ZA at 1050 °C during 4 h and corroded in 35.59 wt.% $MgCl_2$ – 64.41 wt.% KCl at 700 °C in flowing Ar [3].

Immersion time, h	In702 R_p, Ω	j_{corr}, mA/cm^2	Corrosion rate, μm/yr	HR224 R_p, Ω	j_{corr}, mA/cm^2	Corrosion rate, μm/yr
2	375	32	97	119	60	185
8	874	14	42	114	63	193
24	871	14	42	224	32	99
48	400	30	91	107	67	206
72	267	45	136	90	80	244
120	–	–	–	78	92	283

tested with the low oxygen content remaining in the molten salt tested.

Using this thermal purification treatment, the aim of this paper is to analyse different container materials than could be proposed in the new generation of CSP plant containing chloride molten salts.

2. Experimental procedure

The molten salt tested was the eutectic mixture composed by 20.4 wt.% KCl + 55.1 wt.% $MgCl_2$ + 24.5 wt.% NaCl (Sigma Aldrich 99%), at 720°C under inert atmosphere (N_2).

Some analysis were carried out in the commercial salts used in this research (Table 2):

The salts were carefully handled and mixed to avoid water absorption in a dry box containing desiccants and after the thermal purification treatment the salt was solidified and the bottom part was removed, with the insoluble impurities. After thermal purification treatment, electrodes with the alloys to be tested were immersed in the chloride salt at 720 °C. This procedure has been repeated for each material to be tested.

A two electrodes arrangement was used, composed by a working electrode (WE) and reference-counter (RE-CE) electrodes, that were immersed in the molten salt (electrolyte) and the open circuit potential (OCP) was measured using a potentiostat (Gamry 1010E). The experimental set up is shown in Fig. 1.

Electrochemical impedance spectroscopy tests were carried out at 1, 3 and 5 h of immersion to monitor the corrosion mechanism. After 8 hours of immersion, linear polarization tests were performed from a potential of −0.6–0.4 V of the OCP voltage using a scanning range of 0.005 V/s with steps of 0.00244 V.

A specific thermal treatment during the melting process was defined in a previous research [13] in order to reduce the corrosive impurities present in commercial chloride molten salts, especially in $MgCl_2$. The easiest way to prevent the contamination of O_2 and H_2O is to thoroughly dry the hygroscopic $MgCl_2$ salt and parameters for the purification treatment were determined from the vapour-pressure curve of hydrated $MgCl_2$.

Isothermal steps and dwelling times are: 70 °C (2 h)–117 °C (2 h)–145 °C (4 h)–190 °C (4 h)–227 °C (4 h)–300 °C (4 h)–450 °C (3 h)–600 °C (1 h)–720 °C.

These thermal purification treatments are key for corrosion mitigation in chloride molten salts and a pre-treatment tank would be necessary in the industrial scale in order to purify these salts before move them to the storage block.

Materials corrosion screening tests were carried out after this thermal purification treatment in three different alloys, with a chemical composition showed in Table 3.

Table 2
Chemical composition of ternary chloride salt tested.

K (%)	Mg (%)	Na (%)	Mn (ppm)	SO_4 (ppm)	Cl (%)	H_2O (%)
20.6	11.9	3.4	1.8	162	60	5

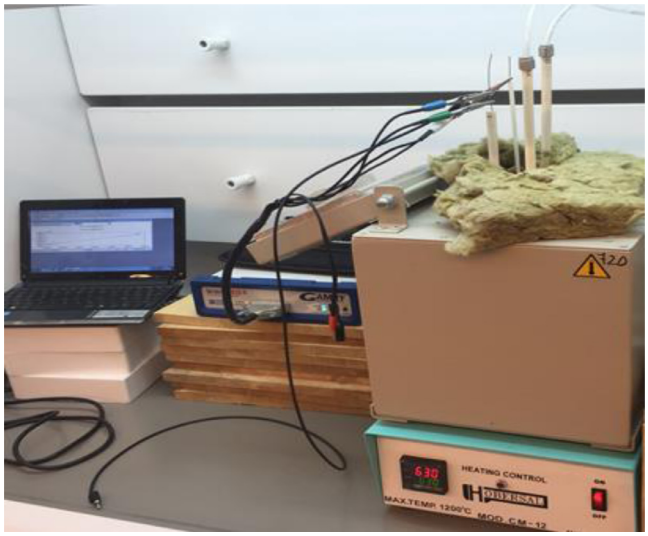

Fig. 1. Experimental setup of electrochemical test in controlled atmosphere.

Table 3
Chemical composition of alloys tested.

Alloys	wt.% Si	Mn	Cr	P	C	S	Ni	Al	Fe
304	0.75	2	18	0.045	0.08	0.03	8	-	Balance
In702	-	-	16	-	-	-	75	3	2
HR224	-	-	21	-	-	-	47	3.2	27.5

After corrosion test, samples were cleaned with hot distilled water and coupons were cooled slowly and then dried. For SEM characterization, they were immersed in a polymer resin prepared by mixing KEM 90 Harz resin and KEM 90 Harter catalyst, in 2:1 proportion. After the resin cured, the samples were manually grinded and polished using SiC abrasive papers (water-based grinding procedure) and diamond power, respectively. The oxidation/corrosion layer of the samples was analysed and its thickness measured by means of a Quanta 200 FEG SEM operated in high vacuum mode at 30 kV equipped with a back-scattered electron detector. EDX analyses were carried out to obtain the chemical composition maps with a recommended working distance around 10 mm.

For XRD analysis, a *PANalytical X'Pert PRO MPD θ/θ* Bragg-Brentano powder diffractometer of 240 mm of radius was used. Tests were carried out using a grazing incidence from 5 to 120° with a step size of 0.017° and a measuring time of 50 s per step.

Electrochemical techniques were used to monitor the corrosion mechanism in the materials tested. For this purpose, a electrochemical impedance test was carried out using the most common equivalent circuit used to model corrosion of bare metal, the Randles circuit [15]. The model can be used to estimate the polarization resistance from the impedance data [16].

Nyquist plots are used to represent the real part of the impedance on the abscissa and the imaginary part thereof on the ordinate axis, both at different frequencies [17]. The semicircle obtained in the parallel RC circuit is used at higher values of Z' and represents the total impedance (Z) of the Randles circuit as:

$$Z = R_S + \frac{1}{\frac{1}{R_{ct}} + j\omega C_{dl}} \quad \text{(I)}$$

where R_s is the resistance of the solution, R_{ct} is the resistance to charge transfer, $j\omega$ is the imaginary radial frequency and C_{dl} is the capacitance

of the double layer.

Different authors [17–22] proposed equivalent circuits that match to the main corrosion processes obtained in a molten salt environment at high temperature, obtaining different case scenarios, a localized corrosion model, porous layer or protective layer model.

After the EIS tests, a linear polarization resistance (LPR) test was carried out. In this case, it is important to quantify the polarization resistance, R_p, to take into account the potential drop attributed to the electrolyte resistance (molten salts). The relationship between polarization resistance and corrosion current density, i_{corr}, is given by Eq. (1I):

$$i_{corr} = \frac{B}{R_p} \quad \text{(II)}$$

B is an electrochemical constant calculated theoretically according to the Eq. (III):

$$B = \frac{\beta_\alpha \cdot \beta_c}{2,3 \cdot (\beta_\alpha + \beta_c)} \quad \text{(III)}$$

where β_c and β_α are the cathodic and anodic Tafel slope, respectively.

The corrosion density current, i_{corr}, and the corrosion potential, E_{corr}, were determined from the extrapolation of the Tafel curve.

The corrosion rate (CR) can be estimated through the Butler-Volmer equation showed in Eq. IV:

$$CR = \frac{i_{corr} \cdot K}{\rho_{alloy} \cdot \sum \left(\frac{f_i \cdot n_i}{MW_i} \right)} \quad \text{(IV)}$$

where K is a correlation constant that defines the units of CR (3272 for CR in mm/year), ρ_{alloy} is the alloy density (g/cm^3), f_i is the mole fraction of the element i in the alloy, n_i is the number of electrons that are transferred in element i and MW_i is the atomic weight of element i.

3. Results and discussion

Nyquist plots obtained for AISI 304 stainless steel are shown in Fig. 2. Results were fitted to a protective layer model at 1 hour of immersion and the corrosion mechanism evolve to a porous layer model at 3 and 5 h of immersion.

It is important to highlight that diffusion direction of oxidants influence the corrosion process since the modulus of the Warburg resistance, related to the solubility and diffusion coefficient of oxidants in the melt, is included in the equivalent circuit (W1). Equivalent circuit element values for this material, are shown in Table 4. These results were confirmed by SEM analysis after immersion test (Fig. 3), obtaining a porous layer with Fe-Cr-Mg-O content.

Nyquist plots for HR224 alloy are shown in Fig. 4. The equivalent circuit obtained at 1 hour (blue line) of immersion showed a localized corrosion model, nevertheless, after 3 and 5 hours a protective corrosion model was detected. Results for equivalent circuits elements are shown in Table 5. These results were confirmed by SEM (Fig. 5), obtaining an internal oxidation (B analysis Fig. 5 right) with higher Cr content. The outer layer in alloy surface showed the formation of a protective layer formed by Fe-Cr-Al-O. It is important to highlight this behaviour since this internal oxidation could be a potential problem for mechanic failures. For this reason, the corrosion layer in this case also must show the inner and outer layers, obtaining 31.5 microns of thickness. According with the EDS analysis performed and the XRD analysis obtained in Table 7, the composition of these layers could be $MgCr_2O_4$ for the internal oxidation and a mix of this compound and Al_2O_3 in the most external layer.

Last material tested was In702, showing a similar behaviour as the previous one, obtaining a localized corrosion model at 1 hour of immersion in ternary chloride molten salt and a protective layer corrosion model up 3 hours of corrosion test. Nyquist plots and equivalent circuits elements are shown in Fig. 6 and Table 6. The corrosion mechanisms obtained at the end of the immersion test were confirmed by SEM (Fig. 7). In this case, a protective layer of 8.93 μ with content in Fe-Ni-Cr-O-Al was detected. In this case, no internal corrosion was detected in the alloy and it could be an interesting alloy for longer exposure times in the corrosive environment testes.

In order to confirm the corrosion layer composition obtained in the materials surface, a XRD analysis was carried out in all the materials tested (Fig. 8). The chemical compounds obtained in the alloys immersed in chloride molten salts along with the different thermal treatment performed are shown in Table 7. Protective layers, with Al and Cr content, were obtained for HR224 and In702, confirming the better corrosion resistance obtained in these materials in contact with

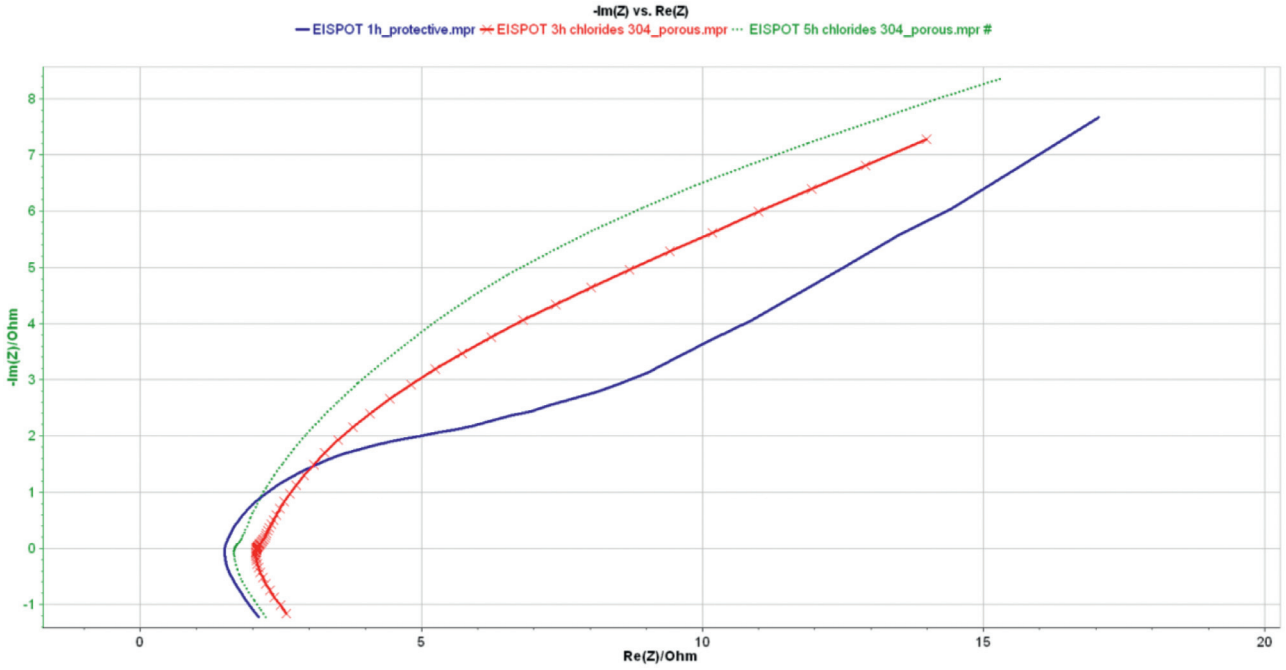

Fig. 2. Nyquist diagram of AISI 304 immersed in ternary chloride molten salt at 1, 3 and 5 h.

Table 4
Electrochemical parameters obtained for EIS tests in AISI304.

Element	R1 (Ohm)	Q2 (F/s)	R2 (Ohm)	W1	Q3 (F/s)	R4 (Ohm)	Equivalent circuit
1 h	1.451	0.486	59.47	-8.775	0.075	4.073	
Element	**R1 (Ohm)**	**Q1 (F/s)**	**R3 (Ohm)**	**R5 (Ohm)**	**W1**	-	
3 h	2.177	0.146	46.68	8.076	3.349	-	
5 h	1.713	0.153	47.28	11.34	4.371	-	
Element (wt.%)	Fe	Cr	Mg	O	Cl		
A	69.28	24.14	0.85	3.57	1.85		
B	72.92	20.49	2.78	3.81	-		
C	3.78	21.25	51.40	21.48	2.10		

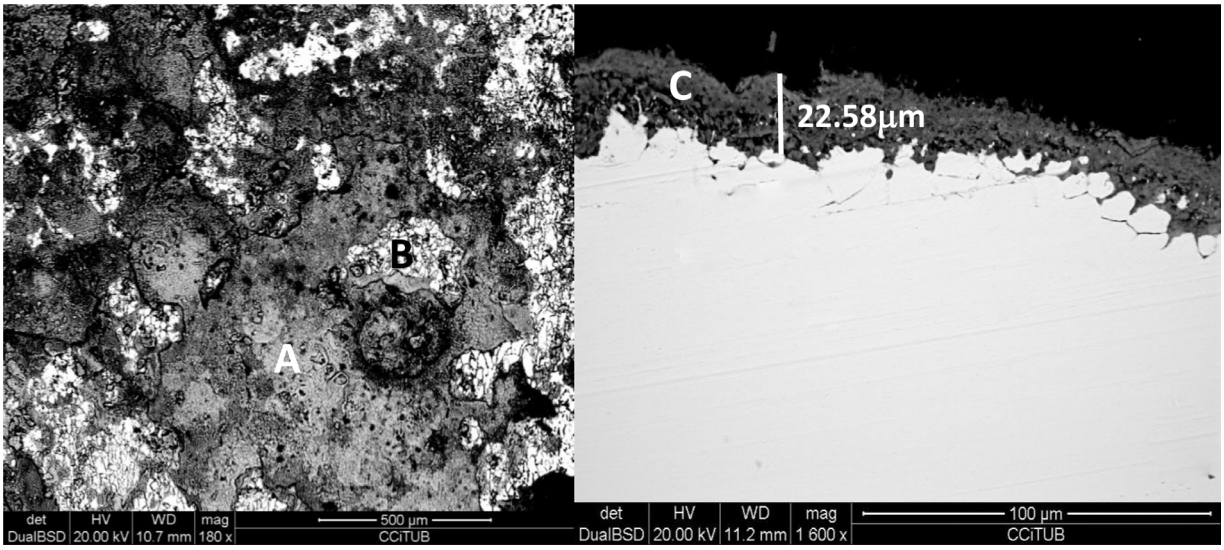

Fig. 3. Top view (left) and cross section (right) images for AISI 304 immersed in ternary chloride molten salt during 8 h at 720 °C and EDX analysis.

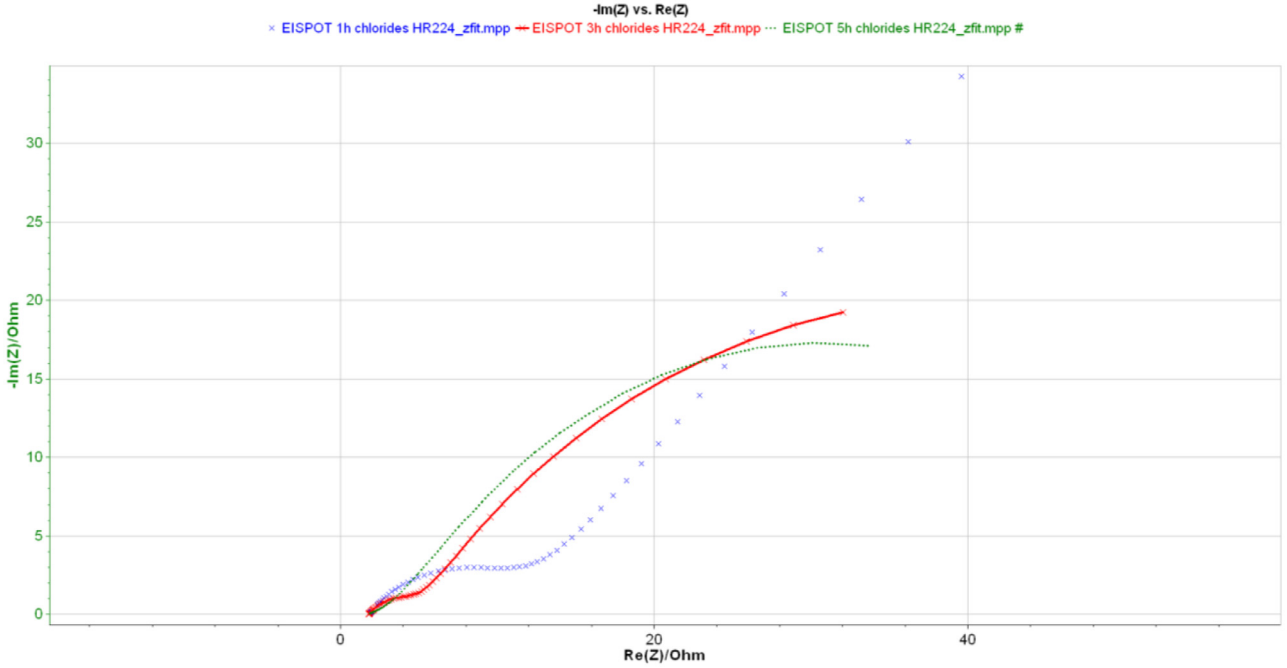

Fig. 4. Nyquist diagram of HR224 immersed in ternary chloride molten salt at 1, 3 and 5 h.

Table 5
Electrochemical parameters obtained for EIS tests in HR224 alloy.

Element	R1 (Ohm)	Q2 (F/s)	R2 (Ohm)	Q3 (F/s)	R3 (Ohm)	Equivalent circuit
1 h	1.812	4.87e-3	11.06	0.104	0.144	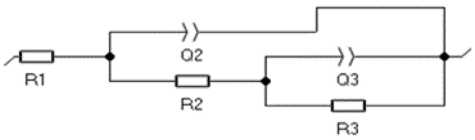
Element	**R3 (Ohm)**	**Q1 (F/s)**	**R5 (Ohm)**	**Q2 (F/s)**	**R7 (Ohm)**	
5 h	1.71	0.166	55.4	0.257	74.11	
3 h	1.785	0.014	3.293	0.123	72.56	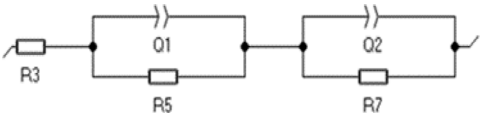

Element (wt.%)	Fe	Cr	Mg	O	Cl	Al	Ni
A	20.73	12.74	34.72	6.87	17.6	1.74	5.61
B	16.05	19.47	1.87	3.14	4.45	2.24	15.7
Element (wt.%)	Fe	Cr	Ni	Mg	O	Cl	Al
A	25.70	43.37	-	4.51	17.9	4.14	4.33
B	1.24	62.57	23.82	2.29	9.22	-	0.86

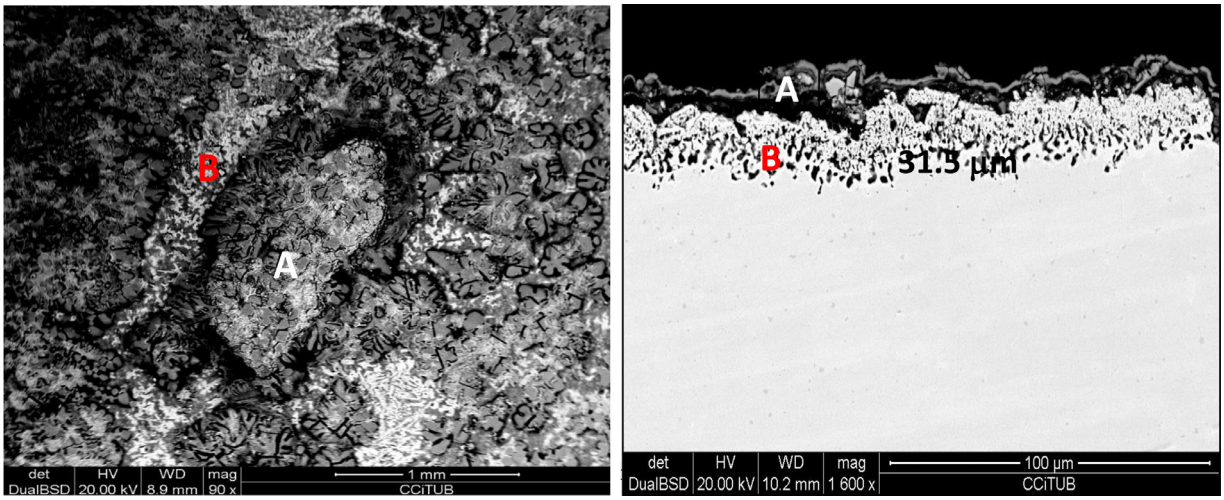

Fig. 5. Top view (left) and cross section (right) images for HR224 immersed in ternary chloride molten salt during 8 h at 720°C and EDX analysis

chloride molten salt and the corrosion mechanism detected by EIS and SEM.

The Tafel curve obtained in AISI 304 is shown in Fig. 9. Fig. 9 shows the fitted carried out to obtain these electrochemical parameters related with the corrosion rate assessment. Materials screening test results are shown in Table 8.

The linear polarization resistance technique was applied in the materials at 720 °C after 8 h of immersion, obtaining a corrosion rate of 8.19, 3.12 and 6.34 mm/year for AISI304, HR224 and In702, respectively.

The lowest corrosion rate was obtained for HR224 in concordance with EIS results (protective layer model) and XRD/SEM results, where a protective layer formed by Al_2O_3 and $MgCr_2O_4$ were detected in the steel surface, however, the SEM analysis (Fig. 5) showed an internal oxidation in the alloy that can produce mechanic failures so this behaviour needs to be monitorized at longer exposure times, since this can evolve to an intergranular corrosion. Results obtained have been used for a down selection of materials and longer exposure times will be performed in the materials with better corrosion rates, in this case HR224 and In702.

4. Conclusions

Once a specific thermal treatment was selected in the first part of this study to purify these salts before a corrosion test, a materials screening test was developed in this second part of the study in order to propose materials for the new generation of CSP plants containing chloride molten salts.

The linear polarization resistance technique was successfully applied in the materials tested and a down selection of materials was complete. The lower corrosion rates were obtained for HR224 and In702 alloys, detected by electrochemical impedance spectroscopy and confirmed by SEM and XRD analysis. It is important to highlight that HR224 alloy showed an internal oxidation composed by $MgCr_2O_4$, detected by XRD analysis and a mix of this compound and Al_2O_3 in the most external layer. Longer exposure times will be carried out in HR224 alloy and if this behaviour is extended, the alloy will be disregard for a commercial application since it can produce intergranular corrosion and hence mechanic failure.

The electrochemical impedance spectroscopy used in this work for down selection of alloys is a rapid selection method, but this method is not sensitive to the corrosion layer morphology (e.g.: internal oxidation). Therefore, this method should be accompanied by SEM/EDS analysis to confirm the corrosion mechanism proposed and the selection of the corrosion resistant alloys, during the chloride molten salts exposure.

Author contribution

Term/Author	Angel G. Fernández	Luisa F. Cabeza

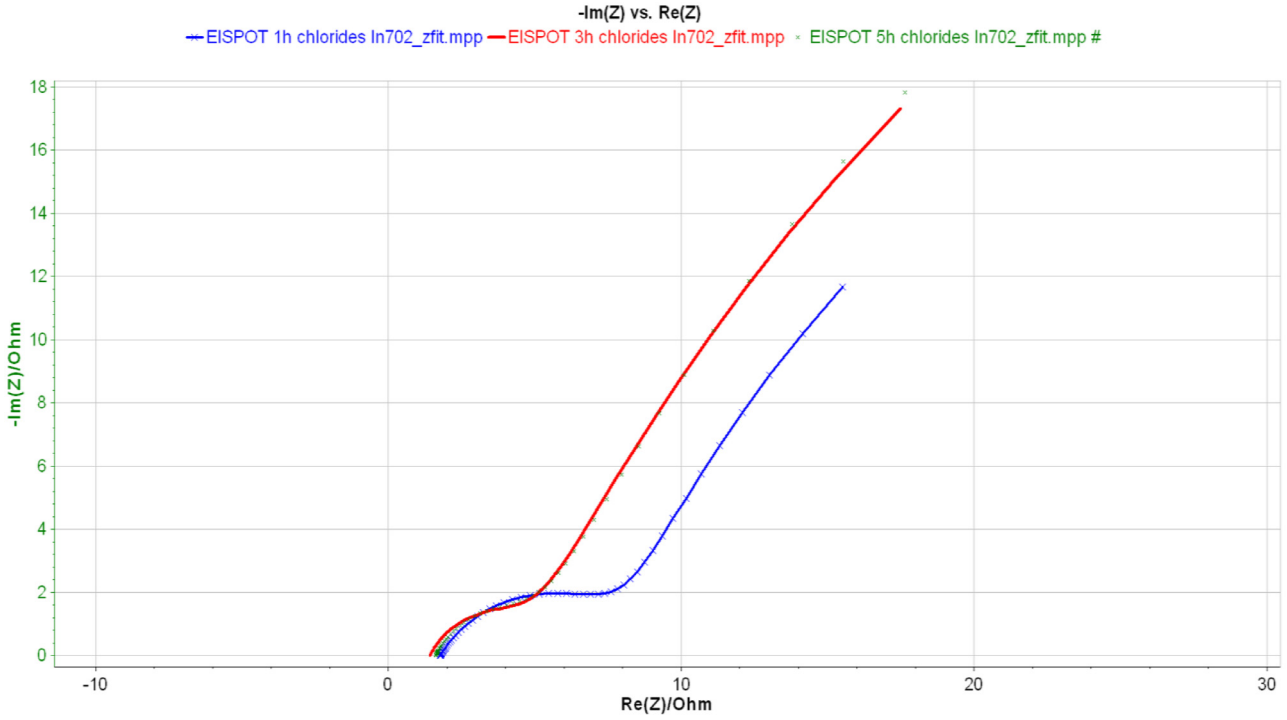

Fig. 6. Nyquist diagram of In702 immersed in ternary chloride molten salt at 1, 3 and 5 h.

Table 6
Electrochemical parameters obtained for EIS tests in In702 alloy

Element	R1 (Ohm)	Q2 (F/s)	R2 (Ohm)	Q3 (F/s)	R3 (Ohm)	Equivalent circuit
1 h	1.762	0.026	7.029	0.484	69.58	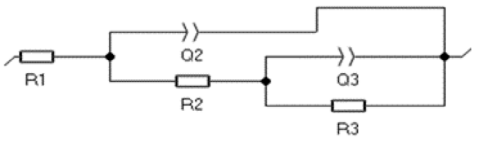
Element	R3 (Ohm)	Q1 (F/s)	R5 (Ohm)	Q2 (F/s)	R7 (Ohm)	
3 h	1.421	0.301	107.6	0.034	3.472	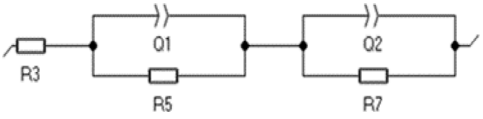

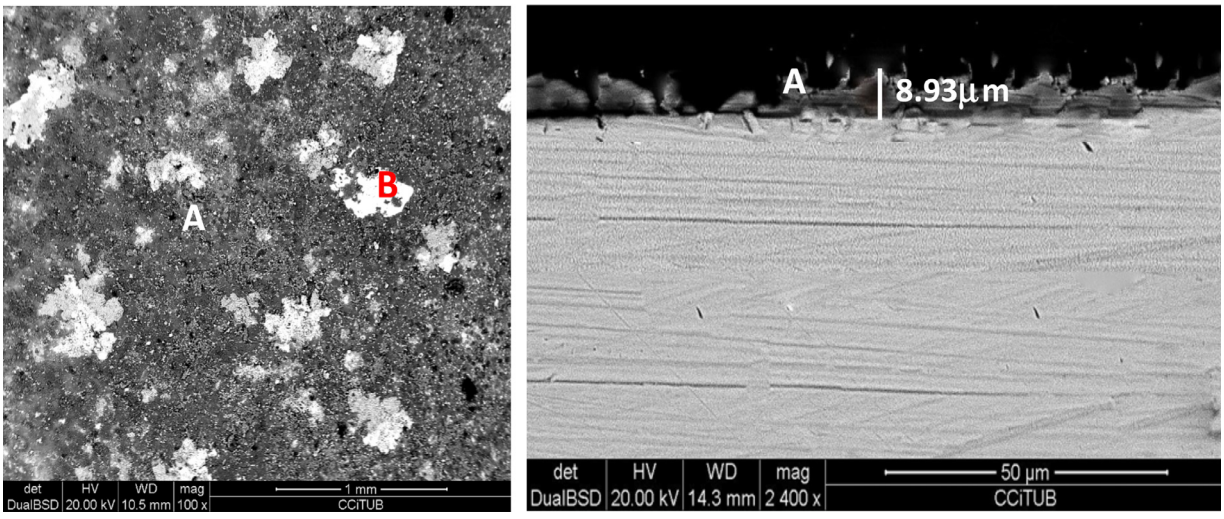

Fig. 7. Top view (left) and cross section (right) images for In702 immersed in ternary chloride molten salt during 8 h at 720 °C and EDX analysis.

Conceptualization	x		Software	x	
Methodology	x	x	Validation	x	x

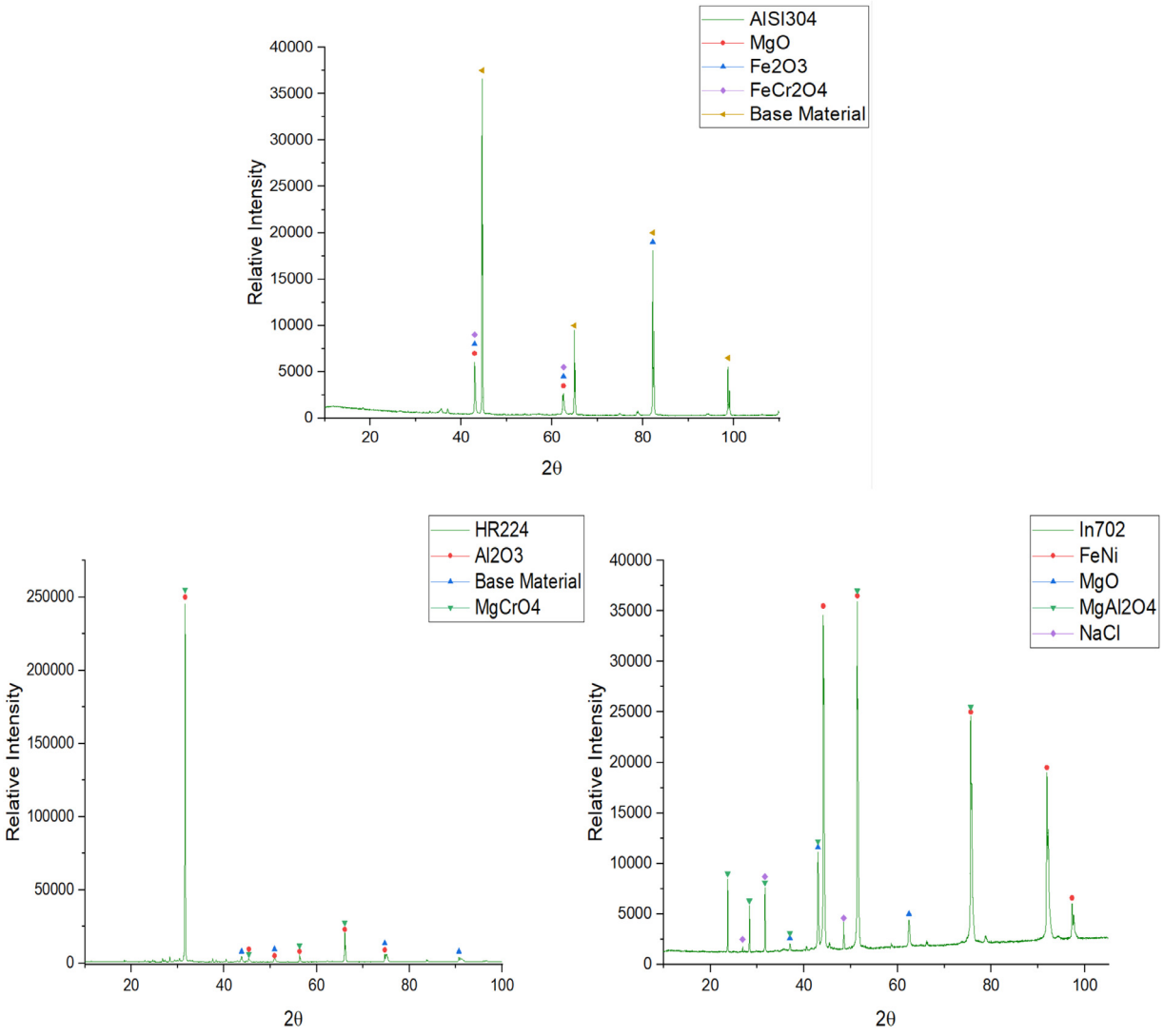

Fig. 8. XRD obtained in AISI304, HR224 and In702 after 8 h of immersion in 20.4 wt.% KCl + 55.1 wt.% $MgCl_2$ + 24.5 wt.% NaCl at 720 °C.

Table 7
Corrosion products identified by XRD analysis on AISI304, HR224 and In702 after exposure to the salt mixture at 720 °C for 8 h.

Salt mixture	Material	Corrosion Products	Reference Pattern
$MgCl_2$/NaCl/KCl (55.1 wt.%–24.5 wt.%–20.4 wt.%)	AISI304	Fe_2O_3 MgO $FeCr_2O_4$	01-089-0597 01-087-0651 00-024-0511
	HR224	Al_2O_3 $MgCr_2O_4$	00-047-1292 00-021-1256
	In702	$MgAl_2O_4$ MgO NaCl	00-033-0853 01-087-0651 00-005-0628

Formal analysis	x	x
Investigation	x	x
Resources	x	x
Data curation	x	
Writing – Original draft	x	
Writing – Review & Editing	x	x
Visualization	x	
Supervision		x
Project administration	x	x
Funding acquistion	x	x

Declaration of Competing Interests

The authors declare that they have no known competing financial interests or personal relationships that could have appeared to influence the work reported in this paper.

Acknowledgements

Angel G. Fernández wants to acknowledge the financial support from the European Union's Horizon 2020 research and innovation programme under the Marie Sklodowska-Curie grant No 712949 (TECNIOspring PLUS) and from the Agency for Business Competitiveness of the Government of Catalonia. This work was partially funded by the Ministerio de Ciencia, Innovación y Universidades de España(RTI2018-093849-B-C31- MCIU/AEI/FEDER, UE). The authors would like to thank the Catalan Government for the quality accreditation given to their research group GREiA (2017 SGR 1537). GREiA is a certified agent TECNIO in the category of technology developers from the Government of Catalonia. This work is partially supported by ICREA under the ICREA Academia programme.

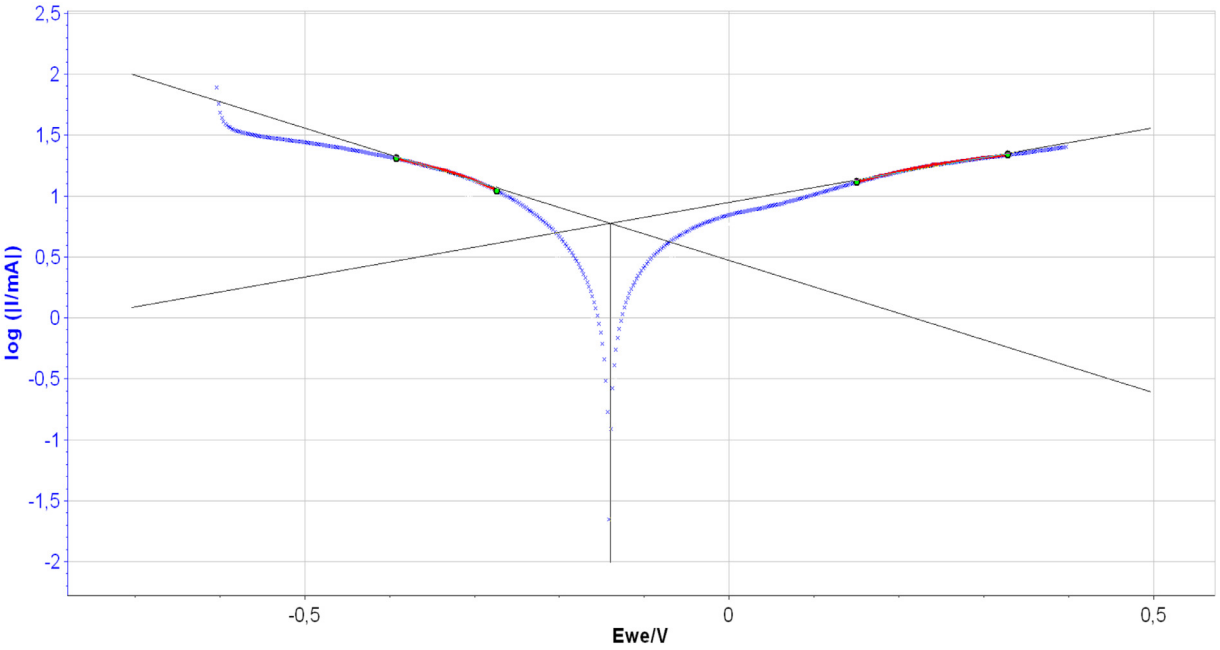

Fig. 9. Tafel curve obtained for the LPR test in AISI304 after 8 h of immersion in chloride molten salt at 720 °C.

Table 8
Electrochemical parameters and corrosion rates obtained for LPR test in the materials tested.

Alloys	Ecorr (mV)	Icorr (mA)	bc (mV)	ba (mV)	A (cm^2)	CR (mm/year)
AISI304	−56.63	4365.86	278.8	856.5	4.25	8.19
HR224	−97.609	2442.67	336.1	325.7	6.75	3.12
In702	−197.78	2876.55	338.6	1021.9	4.26	6.34

Supplementary materials

Supplementary material associated with this article can be found, in the online version, at doi:10.1016/j.est.2020.101381.

References

[1] M. Mehos, J.Vidal C.T., M. Wagner, Z. Ma, C. Ho, W. Kolb, C. Andraka, A. Kruizenga, Concentrating Solar Power Gen3 Demonstration Roadmap, (2017) Technical Report, NREL/TP-5500-67464.
[2] A.G. Fernandez, L.F. Cabeza, Corrosion monitoring and mitigation techniques on advanced thermal energy storage materials for CSP plants, Sol. Energy Mater. Sol. Cells 192 (2019) 179–187.
[3] J.C. Gomez-Vidal, A.G. Fernandez, R. Tirawat, C. Turchi, W. Huddleston, Corrosion resistance of alumina-forming alloys against molten chlorides for energy production. I: Pre-oxidation treatment and isothermal corrosion tests, Sol. Energy Mater. Sol. Cells 166 (2017) 222–233.
[4] J.C. Gomez-Vidal, A.G. Fernandez, R. Tirawat, C. Turchi, W. Huddleston, Corrosion resistance of alumina forming alloys against molten chlorides for energy production. II: Electrochemical impedance spectroscopy under thermal cycling conditions, Sol. Energy Mater. Sol. Cells 166 (2017) 234–245.
[5] K. Vignarooban, Vapor pressure and corrosivity of ternary metal-chloride molten-salt based heat transfer fluids for use in concentrating solar power systems, Appl. Energy 159 (2015) 206–213.
[6] A.M. Kruizenga, Corrosion Mechanisms in Chloride and Carbonate Salts, Sandia Report, 2012 SAND2012-7594.
[7] J.C. Gomez-Vidal, R. Tirawat, Corrosion of alloys in a chloride molten salt (NaCl-LiCl) for solar thermal technologies, Sol. Energy Mater. Sol. Cells 157 (2016) 234–244.
[8] H. Sun, P. Zhang, J. Wang, Effects of alloying elements on the corrosion behavior of Ni-based alloys in molten NaCl-KCl-MgCl2 salt at different temperatures, Corros. Sci. 143 (2018) 187–199.
[9] W. Ding, A. Bonk, T. Bauer, Corrosion behavior of metallic alloys in molten chloride salts for thermal energy storage in concentrated solar power plants: a review, Front. Chem. Sci. Eng. 12 (2018) 564–576.
[10] S.S. Raiman, S. Lee, Aggregation and data analysis of corrosion studies in molten chloride and fluoride salts, J. Nucl. Mater. 511 (2018) 523–535.
[11] Y. Hosoya, T. Terai, T. Yoneoka, S. Tanaka, Compatibility of structural materials with molten chloride mixture at high temperature, J. Nucl. Mater. 248 (1997) 348–353.
[12] W. Ding, H. Shi, Y. Xiu, A. Bonk, A. Weisenburger, A. Jianu, T. Bauer, Hot corrosion behavior of commercial alloys in thermal energy storage material of molten MgCl2/KCl/NaCl under inert atmosphere, Sol. Energy Mater. Sol. Cells 184 (2018) 22–30.
[13] A.G. Fernandez, L.F. Cabeza, Corrosion Evaluation of Eutectic Chloride Molten Salt for New Generation of CSP Plants. Part 1: thermal treatment assessment, J. Energy Storage 27 (2020) 101125.
[14] N. Klammer, C. Engtrakul, Y. Zhao, Y. Wu, J. Vidal, Method to Determine MgO and MgOHCl in Chloride Molten Salts, 92 Analytical chemistry, 2020, pp. 3598–3604.
[15] D.D. Macdonald, Reflections on the history of electrochemical impedance spectroscopy, Electrochim. Acta 51 (2006) 1376–1388.
[16] A. Kisza, The capacitance of the diffuse layer of electric double layer of electrodes in molten salts, Electrochim. Acta 51 (2006) 2315–2321.
[17] Mark E. Orazem, An integrated approach to electrochemical impedance spectroscopy, Electrochim. Acta 53 (2008) 7360–7366.
[18] C.L. Zeng, W. Wang, W.T. Wu, Electrochemical impedance models for molten salt corrosion, Corros. Sci. 43 (2001) 787–801.
[19] A.G. Fernández, A. Rey, I. Lasanta, S. Mato, M. Brady, F.J. Perez, Corrosion of alumina-forming austenitic steel in molten nitrate salts by gravimetric analysis and impedance spectroscopy, Mater. Corros. 65 (2014) 267–275.
[20] G. Gao, H. Stott, L. Dawson, M. Farrell, Electrochemical monitoring of high temperature molten salt corrosion, Oxid. Met. 33 (1990) 79–94.
[21] C.J. Rao, P. Venkatesh, S. Ningshen, Corrosion assessment of 9Cr-1Mo steel in molten LiCl-KCl eutectic salt by electrochemical methods, J. Nucl. Mater. 514 (2019) 114–122.
[22] J. Titz, G.H. Wagner, W.J. Lorenz, In situ EIS studies of localized corrosion processes in research and industrial practice, Electrochim. Acta 37 (1992) 2309–2320.